Vietnam Journal of Earth Sciences, 46(4), 449-467, https://doi.org/10.15625/2615-9783/21040

Vietnam Journal of Earth Sciences
https://vjs.ac.vn/index.php/jse

Assessing Tropical Cyclone-induced rainfall distributions derived from the TRMM and GSMaP satellite datasets over Vietnam's mainland

Ha Pham-Thanh[1], Hang Vu-Thanh[1], Nga Pham-Thi-Thanh[2,*], The Doan-Thi[2], Thuc Tran-Duy[2], Hao Nguyen-Thi-Phuong[3]

[1]*VNU University of Science, 334 Nguyen Trai, Thanh Xuan, Hanoi, Vietnam*
[2]*Vietnam Institute of Meteorology, Hydrology and Climate Change, 62 Nguyen Chi Thanh, Dong Da, Hanoi, Vietnam*
[3]*Vietnam National Space Center, Vietnam Academy of Science and Technology, 18 Hoang Quoc Viet, Cau Giay, Hanoi, Vietnam*

Received 21 February 2024; Received in revised form 20 May 2024; Accepted 27 June 2024

ABSTRACT

In this study, 169 meteorological stations are used as the "ground truth" to assess the Tropical Rainfall Measuring Mission (TRMM) and Global Satellite Mapping of Precipitation (GSMaP) products in estimating tropical cyclone (T.C.)-induced rainfall over Vietnam's mainland during the 2000-2019 period. Various statistical indices compare two satellite rain datasets with rain gauge observations. In this study, the performance of satellite-based precipitation datasets was investigated for T.C.s affecting the entire Vietnam's mainland, mainly focusing on the position of surface weather stations relative to the landfall and movement directions of the T.C.s. The results indicate that both satellite rain datasets accurately provide the radial distribution of TC-induced rainfall, concentrated within 500 km from the T.C. center, and decreases as the distance from the T.C. center increases. Significantly, the verifications show the close similarity between the TRMM and GSMaP products in estimating TC-induced rainfall. In particular, the assessments considering T.C. intensities and T.C. landing sub-regions suggest that the performance of two satellite rain datasets in evaluating TC-induced rainfall over Vietnam's mainland strongly depends on the intensity of TC-induced rainfall. Light rainfall is estimated more accurately than heavy rainfall. As a result, the performance of the TRMM and GSMaP show higher errors in the coastal areas, where most TC-induced rainfall concentrates, particularly within a 200 km radius of the T.C. center. Besides, M.A.E. exhibits higher values on the left side of the T.C. track compared to those on the right side for all T.C. intensities while showing differences in T.C. landing sub-regions for both datasets.

Keywords: TRMM; GSMaP; TC-induced rainfall; Vietnam's mainland.

1. Introduction

Precipitation datasets with high temporal and spatial resolutions are essential for numerous weather and climate research and practical applications. At the same time, rain gauge data are usually used to evaluate against other data sources and considered the "ground truth". Their accessibility is limited in

*Corresponding author, Email: pttnga.monre@gmail.com

various areas such as oceans, mountain regions, and deserts. Besides that, many gauge stations provide only infrequent measurements, typically recording rainfall amounts at 6-hourly or daily intervals. Compared to rain gauges, weather radar networks offer enhanced spatial and temporal coverage; nevertheless, the accuracy and effectiveness depend significantly on topographic factors, such as mountain blockage. Hence, precipitation data derived from satellites have become a primary solution. These data have been widely used to analyze precipitation features (Nesbitt et al., 2003; Liu et al., 2021; Roy and Rao, 2022), improve the initialization of numerical models (Hou et al., 2001; Bahrami et al., 2023), and verify model predictions/simulations (Ebert et al., 2007; Yue et al., 2022).

Given the high demands of society, several global satellite-based precipitation products have widely used, including TRMM (Huffman et al., 2007), GSMaP (Okamoto et al., 2005; Kubota et al., 2007; Aonashi et al., 2009; Ushio et al., 2009), Climate Prediction Center MORPHing Technique (CMORPH) (Joyce et al., 2004), Precipitation Estimation from Remotely Sensed Information Using Artificial Neural Networks (PERSIANN) (Sorooshian et al., 2000; Ashouri et al., 2015) and Integrated Multi-satellitE Retrievals for Global Precipitation Measurement (G.P.M.) (IMERG) (Huffman et al., 2015). Notably, these datasets rely on indirect methods to estimate precipitation, in contrast to direct measurements obtained by rain gauges. These indirect methods typically use one or more remotely sensed features of clouds, such as scattering effects of raindrops or ice particles (microwave), cloud-top temperature (infrared), and cloud reflectivity (visible) to estimate precipitation extracted from satellites (Kidd and Levizzani, 2011; Deo et al., 2016). Consequently, significant variability is inevitable in satellite-based precipitation data (Derin et al., 2014; Sun et al., 2018). Hence, satellite-based precipitation datasets must be validated with surface-based "ground truth" data, such as rain gauge or radar data. Numerous studies have been done to provide the accuracy and limitations of satellite-based precipitation datasets worldwide.

Some studies have demonstrated that satellite-based precipitation datasets can capture reasonably well T.C. precipitation systems (Nesbitt et al., 2003; Lonfat et al., 2004; Chen et al., 2006; Pham and Vu, 2020; Sutton et al., 2022), and then they were used to analyze T.C. clouds and TC-induced precipitation characteristics (Yu et al., 2009; Huang et al., 2019; Zhao et al., 2022). In particular, Lonfat et al. (2004) used TRMM to determine the spatial precipitation distribution of 260 TCs over the global oceans in the 1998-2000 period. It can be found that the azimuthal mean rain rates are very different from T.C. intensities and oceanic basins. The maximum azimuthal mean rain rate is about 12 mm h^{-1} for CAT35 (T.C.s with winds > 49 m s^{-1}) but declines to 7 mm h^{-1} for CAT12 (T.C.s with winds from 34-48 m s^{-1}) and to 3 mm h^{-1} for tropical storms with wind < 33 mm s^{-1}. Yu et al. (2017) investigated the linkage between T.C. intensity and rainfall distribution using TRMM satellite 3B42 rainfall estimated from landfalling T.C.s over China in 2001-2015. It can be seen that stronger T.C.s typically have higher average total rain, larger average rain areas, and higher average maximum axisymmetric rain rates. The results also showed that the highest total rainfall, largest rain area, and highest rain rate depend on T.C. intensity. Additionally, some studies have evaluated the TRMM Multi-Satellite Precipitation Analysis (TMPA) 3B42 in estimating precipitation during the passage of T.C.s. Yu et al. (2009) used 6 and 24 h precipitation derived from three datasets, namely TRMM 3B42, CMORPH, and

Geostationary Meteorological Satellite-5 infrared brightness temperature (GMS5-TBB), comparing with rain gauge observations during the T.C. periods affecting mainland China in four years from 2003 to 2006. The results showed that all satellite rainfall products have lower skills with higher latitudes and rainfall amounts. The analyses also pointed out that satellite rainfall underestimates moderate and heavy rainfall and vice versa with light rainfall. Chen et al. (2013b) used the Comprehensive Pacific Rainfall Database (PACRAIN) of 24 h rain gauge observations to compare with T.C. rainfall estimation of TRMM 3B42 version 7. They concluded that TRMM 3B42 detects intense T.C. precipitation very well with high correlation and pattern matching with observations. Generally, the heavy rainfall frequency of TRMM 3B42 is overestimated over the ocean but underestimated over land. The results also found that TRMM 3B42 cannot capture high elevation during T.C. landfall, leading to a significant underestimation of T.C.'s heavy rainfall. The study of Deo and Walsh (2016) showed that TMPA has a moderate skill in determining precipitation during the T.C. tracks over Fiji Island. They also found that the higher rainfall intensity values, distance from the T.C. center, and terrain elevation, the lower values of this skill. Such results were also found in some other studies, such as Habib et al. (2009), Chen et al. (2013a,b), Deo et al. (2017); Bagtasa (2022) assessed the accumulated T.C. rainfall estimated from GSMaP and G.P.M. products in the Philippines from 2000 to 2021. The results showed that both the uncalibrated near-real-time GSMaP_NRT and the reanalysis GSMaP_RNL have the worse scores compared to GPM_ER with station correlation coefficient values of 0.63, 0.67, and 0.73, respectively. In the study of Yang et al. (2024), the IMERG V06 and GSMaP products were evaluated for T.C. applications against satellite microwave-derived Goddard Profiling Algorithm (GPROF) rainfall data from 2000 to 2012.

In the western North Pacific (W.N.P.), Vietnam frequently experiences the impact of T.C.s. TC-induced rainfall could account for 25% of the total annual rainfall in Vietnam's coastal regions (Pham-Thanh et al., 2020). In the context of global warming, both the number of solid T.C.s and the lifetime of them affecting Vietnam have been recently increasing (Tran-Quang et al., 2021), consequences as both increases in T.C. rainfall and T.C. heavy rainfall days also documented in some parts of Vietnam (Nguyen-Thi et al., 2012). Undoubtedly, satellite precipitation estimates, offering timely and comprehensive information about TC-induced rainfall patterns, become valuable datasets thanks to their significance across various aspects, such as disaster readiness, agricultural productivity, and water resource management. Trinh-Tuan et al. (2019) validated three satellite precipitation products, including CMORPH, GSMaP, and TRMM 3B42, against the rain gauge-based Vietnam Gridded Precipitation dataset (VnGP) over Central Vietnam during the rainy seasons from 2001 to 2010. The results showed that TRMM showed higher correlations, lower biases, and lower Root Mean Square Error (RMSE) ratios compared to GSMaP and CMORPH for the Vietnam Central Highlands at regional and monthly scales. Besides, GSMaP performed poorly on Vietnam's Central Coast. They also concluded that TRMM performed better than two satellite datasets, especially at rainfall thresholds from 25 to 80 mm day^{-1}. The three datasets could reproduce widespread heavy rainfall days in T.C. and the Inter-tropical Convergence Zone (ITCZ) cases. However, hitherto, no study has investigated the performance of satellite-based precipitation datasets to T.C.s affecting the entire Vietnam region, especially following

the position of surface stations relative to the landfall and movement directions of the T.C.s. A quantitative evaluation of these datasets is essential for understanding their performance and boosting confidence in their use for our further studies on TC-induced rainfall forecasted by statistical models for Vietnam.

Thus, this study aims to provide an initial assessment of the satellite-based rainfall datasets, including TRMM and GSMaP, specifically for TC-induced rainfall landing mainland Vietnam during the 2000–2019 period. Both datasets are compared to rain gauges to evaluate their accuracy concerning (1) T.C. intensities and (2) T.C. landing sub-regions across Vietnam, especially following the position of surface stations relative to the landfall and movement directions of the T.C.s. The rest of this study is organized as follows: Section 2 provides details of datasets and verification methods. Section 3 compares TC-induced rainfall derived from satellite datasets against surface observations and respective discussions. Concluding remarks are summarized in Section 4.

2. Data and Methods

2.1. Data

2.1.1. Tropical cyclone data

The information on 131 TCs landing on Vietnam's mainland during 2000-2019 is collected from the National Centre for Hydro-Meteorological Forecasting of the Viet Nam Meteorological and Hydrological Administration. The data include an identification number, international name, best track, minimum sea level pressure, and maximum wind speed at 6-hour intervals.

2.1.2. Rainfall data from satellites and meteorological surface stations

In this study, two satellite-based rainfall datasets were used. The first dataset is the Global Satellite Mapping and Precipitation moving vector with Kalman filter (GSMaP_MVK, hereafter referred to as GSMaP) algorithm version 6 (product version 3), with a spatial resolution of 0.1 × 0.1 degrees. The GSMaP data is generated by collaborating multiple satellites, including G.P.M. satellites, passive microwave, and infrared radiometers on geostationary satellites (Okamoto et al., 2005; Kubota et al., 2007; Aonashi et al., 2009; Ushio et al., 2009). Furthermore, data sourced from the TRMM 3B42 Version 7, referred to as TRMM, were also used in this study. The TRMM dataset, available at three-hour intervals, is created from multiple satellites, combining passive microwave and geostationary infrared data for real-time monitoring and subsequent research. The TRMM algorithm involves calibrating and combining microwave rainfall estimates, generating infrared rainfall estimates based on the calibrated microwave data, and then merging the infrared and microwave data (Huffman et al., 2007). In this study, hourly satellite-based datasets are converted to a daily time scale and subsequently interpolated to match the corresponding station locations using the bilinear method.

The rainfall data from 169 surface meteorological stations validate two satellite-derived rainfall datasets during T.C.s' landfall in Vietnam. To address potential biases due to missing data, a methodology similar to that used in a prior study focused on the Vietnam region (Pham-Thanh et al., 2019) was adopted. The distribution of meteorological sites and five landing sub-regions (AR1 to AR5) are demonstrated in Fig. 1. Determining five landing sub-regions follows the regulation of the Ministry of Natural Resources and Environment of Vietnam and is used in operational works.

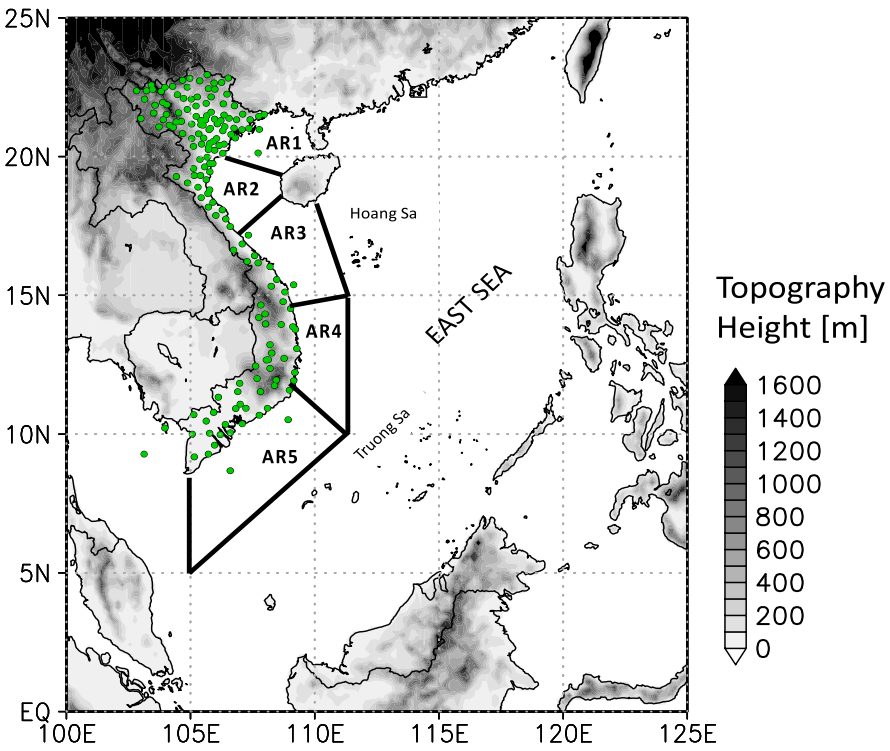

Figure 1. Locations of 169 meteorological surface stations (green points) and 5 landing sub-regions (black lines)

2.2. Verification methods

The performance of TRMM and GSMaP are evaluated depending on different T.C. intensities and 5 landing sub-regions in terms of distance from the T.C. center and position relative to the T.C. *track*. Specifically, two groups for detailed evaluation are divided as follows: (1) Group 1 is based on T.C. intensities (according to World Meteorological Organization classification), including Tropical Storms (T.S.) for cases with maximum wind speeds ranging from 63-88 km/h, Severe Tropical Storm (S.T.S.) for cases with maximum wind speeds ranging from 89-117 km/h, and Typhoon (T.Y.) for cases with maximum wind speeds of >= 118 km/h; (2) Group 2 is based on 5 landing sub-regions labeled as AR1-5, as shown in Fig. 1. The sample number of T.C.s in each group is shown in Table 1.

This study also evaluates the performance of TRMM and GSMaP on both the left and right sides of the T.C. tracks. Figure 2 illustrates the best track of Kaemi TC, where a "red star" indicates the T.C. landing point in the AR3 sub-region. Furthermore, the figure also displays the stations on the right side (green points) and the left side (blue points) of the T.C. track, when a purple circle denotes the T.C. center location. The side determination relies on station positions relative to the current T.C. center (purple circle) and the previous T.C. center (red star). Gray points (N.A.) indicate stations beyond the 500 km radius from the current T.C. center (purple circle).

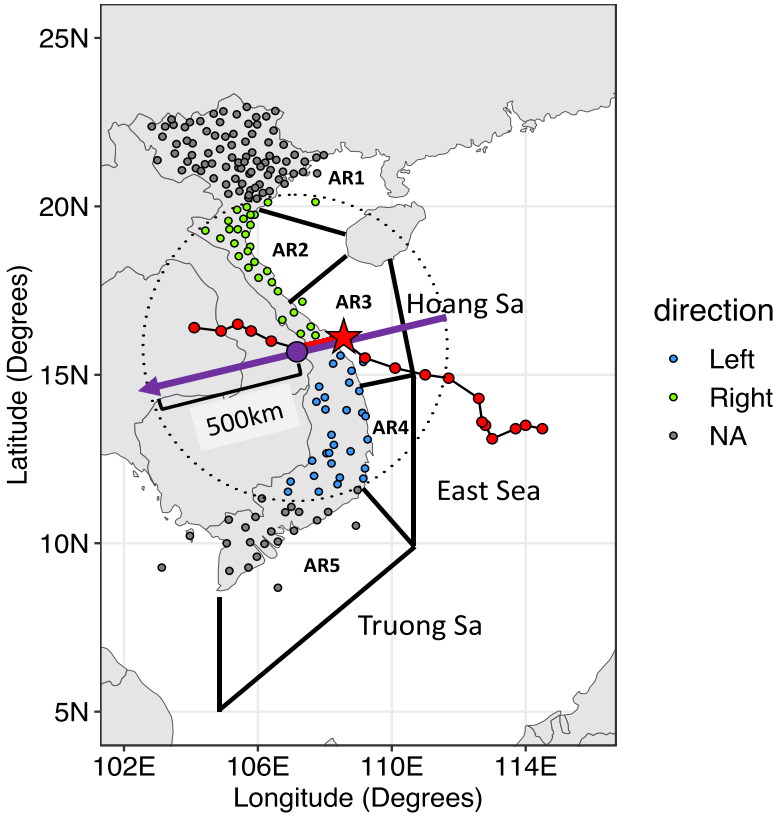

Figure 2. The illustration of the best track of Kaemi TC started from 19/08/2000 to 23/08/2000 and the determination of stations on the left and right sides of the T.C. track

Table 1. The T.C. samples of each category were in two groups

	Category	T.C. samples
Group 1	T.S.	47
	S.T.S.	25
	T.Y.	59
Group 2	AR1	77
	AR2	19
	AR3	7
	AR4	20
	AR5	8

Several statistical indices are used to evaluate the consistency and accuracy of the TRMM and GSMaP datasets. In particular, Mean Error (M.E.) and Mean Absolute Error (M.A.E.) are utilized to assess bias. Categorical statistical indices, including Probability of Detection (P.O.D.), False Alarm Ratio (FAR), Frequency Bias Index (F.B.I.), and Critical Success Index (C.S.I.), which are computed based on a contingency table at different rain thresholds. These categorical statistical indices rely on different rainfall thresholds to determine the distinction between rain and no-rain events, as shown in Table 2. The detailed formulas of these indices are referenced from Wilks, 2006, and are shown in the appendix.

Table 2. Rainfall categories and rainfall thresholds. Column 1 is used for analyzing the bias (e.g., M.A.E.); Column 2 is used for the categorical statistics (e.g., P.O.D., FAR, F.B.I., C.S.I.)

Rainfall categories (mm/day)	Rainfall thresholds (mm/day)
0-5	5
5-15	15
15-30	30
30-45	45
45-60	60
60-75	75
75-100	100

3. Results and discussions

3.1. Ability of satellites to capture the mean radial distribution of T.C. rainfall

Figure 3 shows the radial distribution of mean daily TC-induced rainfall of TRMM, GSMaP, and gauge observation estimated as a function of distance from the T.C. center during the 2000-2019 period. It can be seen that the TRMM and GSMaP rain products capture the radial distribution of observed TC-induced rainfall well. The highest average daily rainfall is within a radius of 100 km from the T.C. center. As the distance from the T.C. center increases, the rainfall gradually decreases. However, once the distance from the T.C. center exceeds 500 km, there is no significant further change in the mean daily rainfall. These results align with previous studies, such as those conducted by Rao and MacArthur (1994), Rodgers et al. (2000), Nguyen-Thi et al. (2012), and Pham-Thanh et al. (2020). Thus, in this study, TC-induced rainfall is defined as the daily rainfall that occurs when the T.C. center is within a 500 km radius of the meteorological station. Additionally, Fig. 3 demonstrates a consistent pattern: the TRMM and GSMaP products tend to underestimate rainfall when the distances from the T.C. center are close (within 100 km), and vice versa. The underestimation of TRMM in estimating T.C. heavy rainfall is also found in the study of Yu et al. (2009) and Chen et al. (2013b).

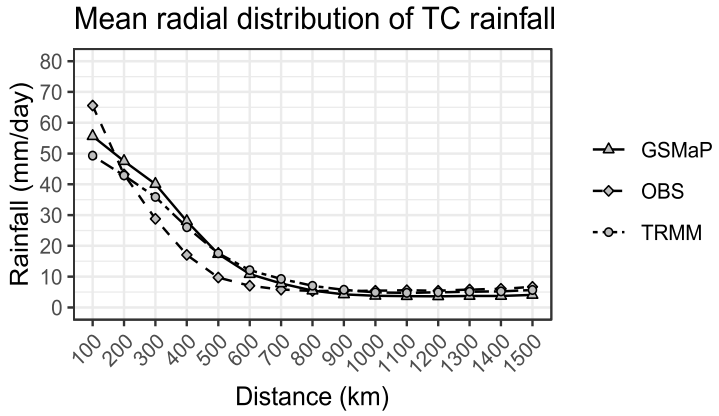

Figure 3. The radial distribution of mean daily TC-induced rainfall of TRMM (circles), GSMaP (triangles), and gauge observation (rhombuses) was estimated as a function of distance from the T.C. center during the 2000-2019 period

3.2. Skills concerning T.C. intensities

Figure 4 displays the spatial distributions of M.E. and M.A.E. of TRMM and GSMaP in evaluating TC-induced rainfall across different T.C. intensity categories, namely T.S., S.T.S., and T.Y., as mentioned in section 2.2. Overall, across all T.C. intensity categories, the spatial patterns of bias errors exhibited by TRMM and GSMaP demonstrate a high level of agreement. In particular, the positive M.E. values are predominant, accounting for at least 66.7% of the stations in the investigated cases. Moreover, the number of stations having positive M.E. values tends to rise as the T.C. intensity increases. However, it is worth mentioning that TRMM shows a higher number of stations with positive M.E. values when compared to GSMaP across all T.C. intensities. The overestimation of TRMM could also be found in the study of Chokngamwong and Chiu (2008), which compared TRMM products with daily rainfall gauges during heavy rainfall events in Thailand. The M.A.E. values tend to be higher along the coast and lower

when far away from the ocean. Additionally, the M.A.E. values are generally higher in the case of weak T.C.s for TRMM and GSMaP compared to those in other T.C. categories.

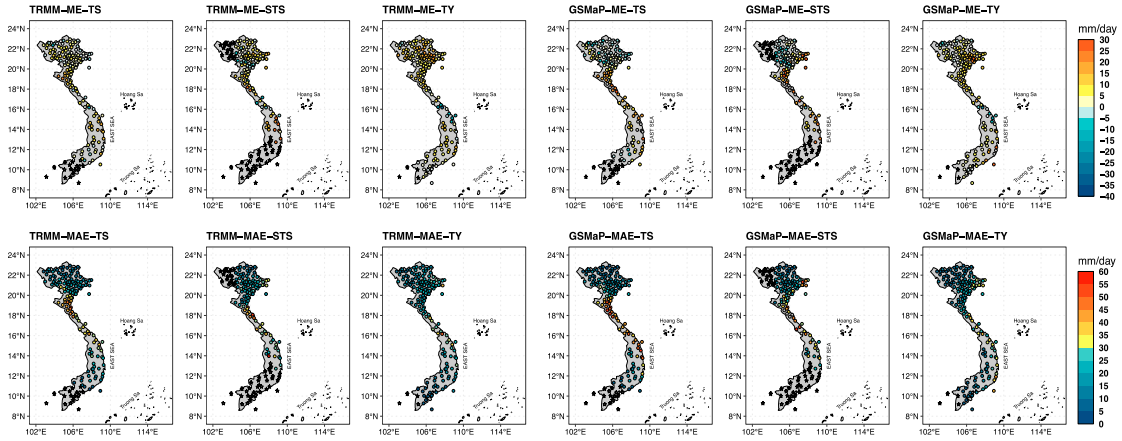

Figure 4. Spatial distributions of M.E. (row 1) and M.A.E. (row 2) for TRMM (columns 1-3 representing T.S., S.T.S., and T.Y. intensity categories, respectively) and GSMaP (column 4-6 representing T.S., S.T.S., and T.Y. intensity categories, respectively). Stars indicate the N.A. values

In Fig. 5, M.E. and M.A.E. mean values are shown separately for the left and right sides of T.C. tracks at different T.C. intensity categories. Overall, the errors of TC-induced rainfall of GSMaP, as represented by both M.E. and M.A.E., are higher than those of TRMM. However, despite the difference in error magnitudes, TRMM and GSMaP display high similarity in their performance. Both satellite datasets tend to overestimate TC-induced rainfall, and the differences between their estimates and observations are more pronounced on the left side of the T.C. tracks than on the right side across all T.C. intensity categories. It is noted that the M.A.E. values increase as the T.C. intensities decrease for both the TRMM and GSMaP datasets, ranging from 17.5 mm/day to 27.5 mm/day. Besides that, Fig. 6 provides further insight into the satellite skills, indicating that these skills strongly depend on the radial distance from the T.C. center. The locations near T.C.s within 200 km, particularly at a distance less than 100 km on the left side of the T.C. track, show higher errors in the performance of both TRMM and GSMaP. These results remain consistent across all investigated T.C. intensity categories for both satellite datasets.

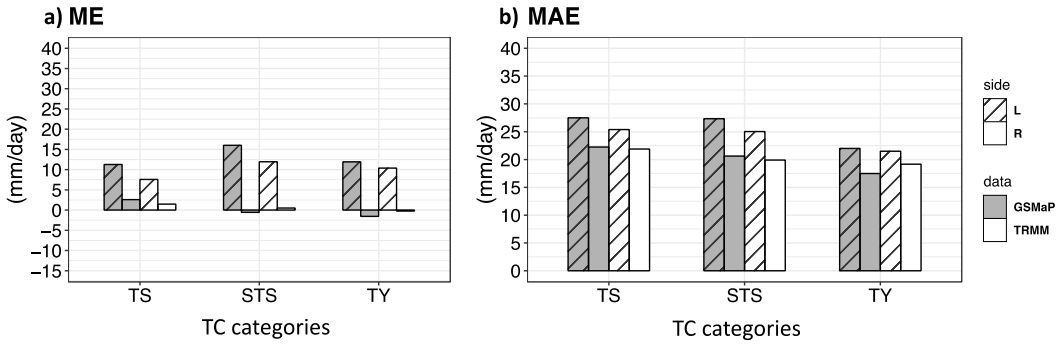

Figure 5. a) M.E. and b) M.A.E. of TRMM (white) and GSMaP (grey) for different T.C. categories to the left side (diagonal pattern) and right side (blank pattern) of the T.C. track

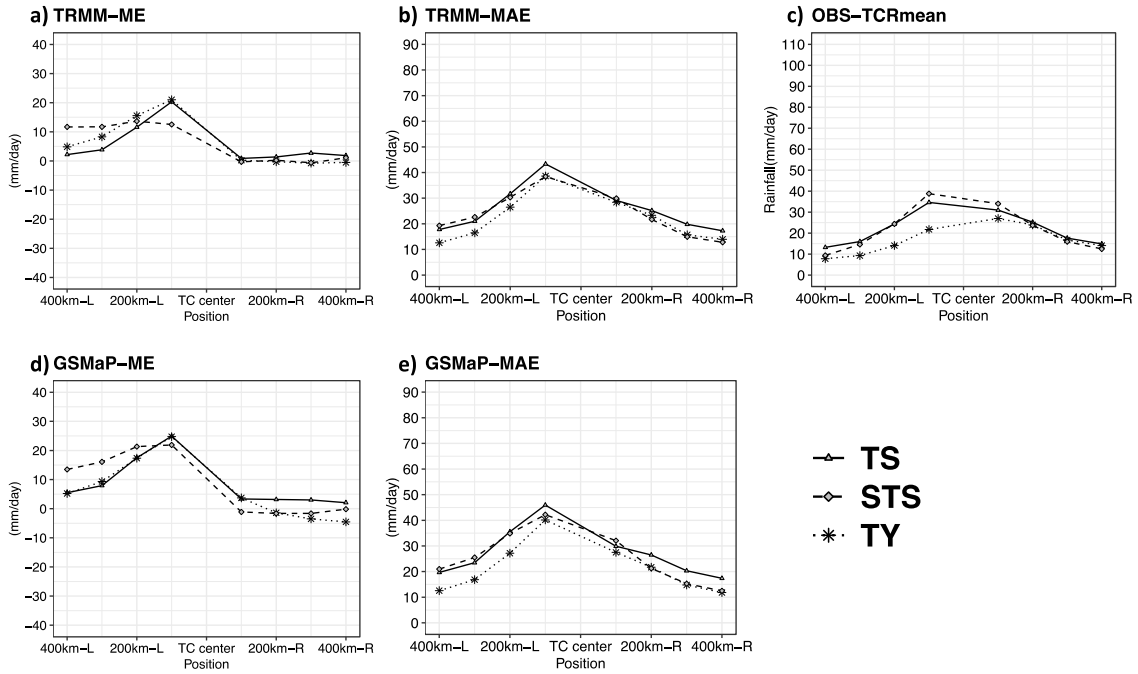

Figure 6. The radial distribution (to the left side (L) and right side (R) of the T.C. center) of: a) M.E. of TRMM; b) M.A.E. of TRMM; c) Mean observed TC-induced rainfall; d) M.E. of GSMaP, e) M.A.E. of GSMaP for T.C. categories including T.S. (triangle), S.T.S. (rhombus), and T.Y. (circle)

3.3. Skills for landing sub-regions

In Fig. 7 and Fig. 8, there is a high similarity in the spatial distributions of M.E. and M.A.E. in cases of T.C. landing sub-regions AR1-5 between TRMM and GSMaP. Overall, for both datasets, the positive M.E. values are dominant for Vietnam's mainland stations, accounting for more than 68% of stations, except for the cases of T.C.s landing in AR3. In particular, the number of stations with negative M.E. values contributes to about 64% and 40% of the stations affected by T.C.s landing in AR3 for TRMM and GSMaP, respectively. Besides that, M.A.E. generally decreases with increasing distance from the coast, irrespective of the TC-landing sub-regions. Notably, the high M.A.E. values exceeding 50 mm/day are located dominantly on the coast of Central Vietnam (AR3-4), consistent with results obtained when analyzing satellite performance for different T.C. intensity categories (Fig. 4). The high M.A.E. values in the coastal Central region suggest the challenges in accurately estimating TC-induced rainfall in this area for both TRMM and GSMaP datasets.

Figure 9 shows the mean values of M.E. and M.A.E. for both sides of the T.C. track at cases of different T.C. landing locations. Overall, for both sides of the T.C. tracks, the TC-induced rainfall data of GSMaP tend to be higher than those of TRMM and observations. For both datasets, M.E.s are consistently higher on the left side than on the right side of the T.C. track for almost all cases of T.C.s landing over Vietnam sub-regions, except for AR3 and AR4. TRMM tends to underestimate TC-induced rainfall of T.C.s landing in AR3, which is clearly noticeable on the right side of the T.C. track (Fig. 9a). Additionally, Fig. 10 reveals the highest bias concentrated in regions closest to the T.C. center (within 200 km), with values decreasing at greater distances. The M.A.E.s of both TRMM and GSMaP exhibit similar performance in 5 T.C.

landing sub-regions (e.g., AR1-5), with the values being relatively close. In general, M.A.E.s tend to be greater on the left side than those on the right side for all T.C. landing locations, except for landing in AR3 and AR4.

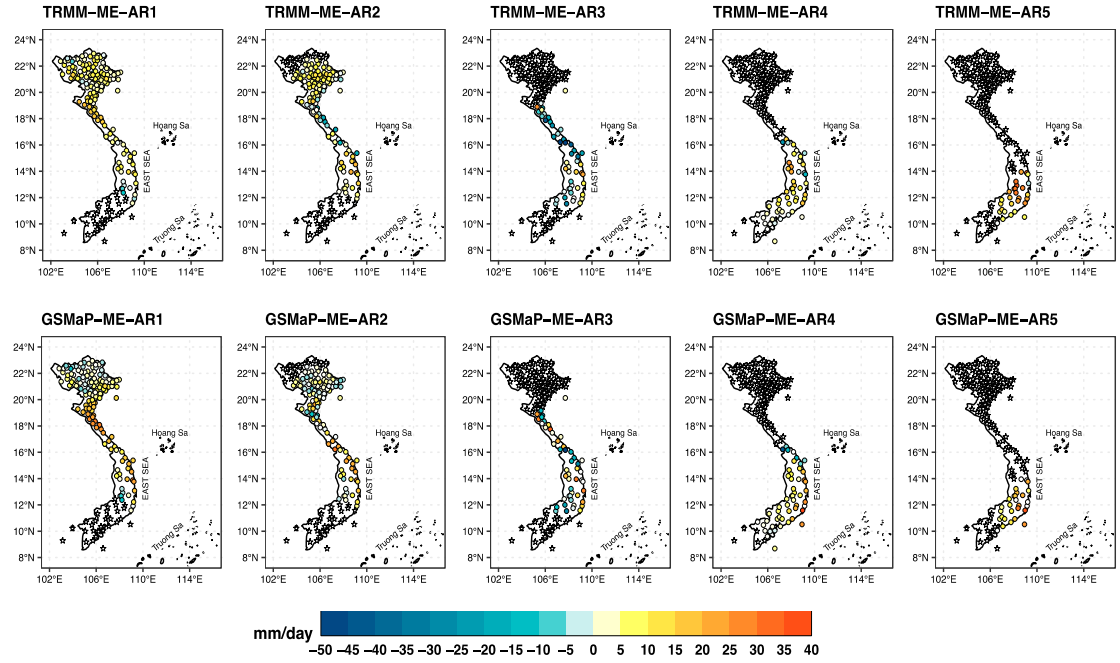

Figure 7. Spatial distributions of M.E. for TRMM data (row 1) and GSMaP data (row 2) in cases of T.C. landing sub-regions: AR1 (column 1), AR2 (column 2), AR3 (column 3), AR4 (column 4), and AR5 (column 5). Stars indicate the N.A. values

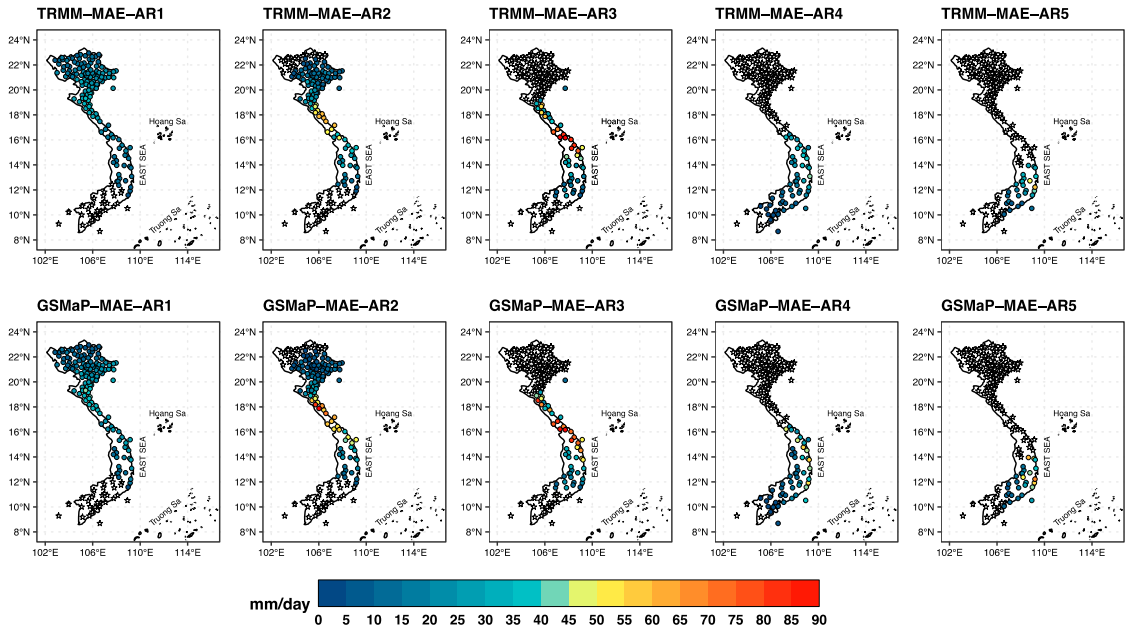

Figure 8. Same as Fig. 7 but for M.A.E.

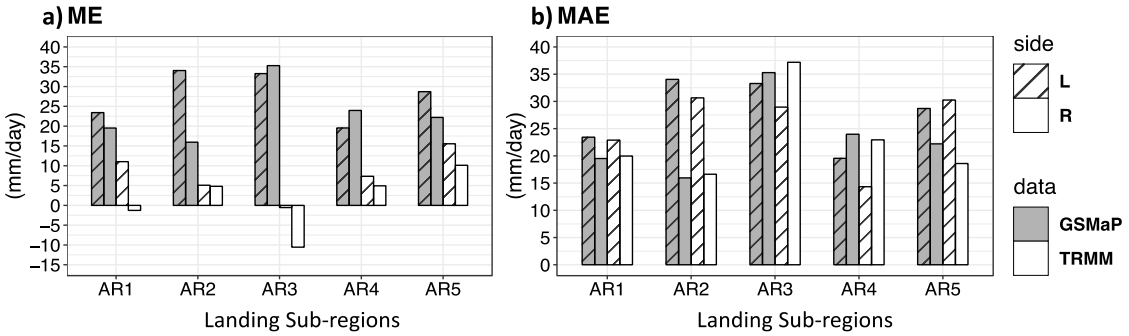

Figure 9. Same as Fig. 5 but for five landing sub-regions

Consistent with the results from Fig. 6, the regions near T.C.s within 200 km, especially at distances below 100 km on the left side, show higher M.A.E.s in both TRMM and GSMaP for all cases of T.C. landing locations (Fig. 10). These results illustrate a strong relationship between the magnitude of M.A.E.s and the observed TC-induced rainfall across all investigated cases, including variations with T.C. intensities and landing sub-regions. Sub-regions with higher M.A.E.s consistently correspond to higher TC-induced rainfall levels, highlighting the influences of TC-induced rainfall intensities on the accuracy of satellite estimates.

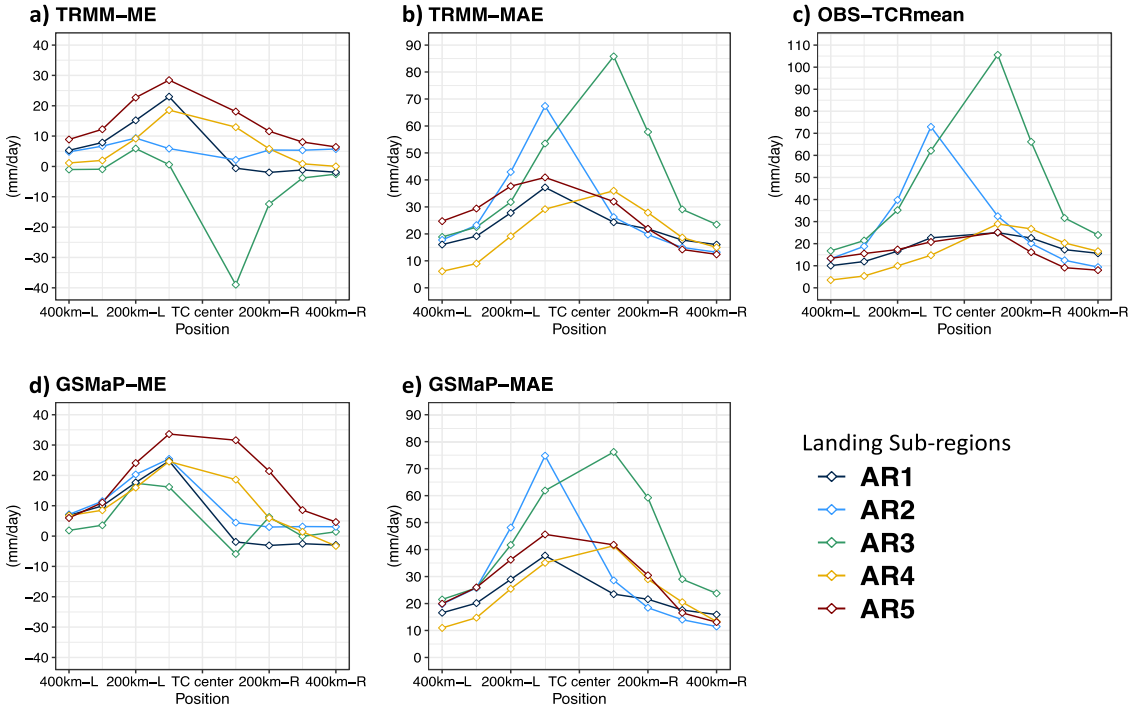

Figure 10. Same as Fig. 6 but for five landing sub-regions

The performance of satellite datasets in estimating the TC-induced rainfall at different rain rates in AR1-5 are presented in Fig. 11 and Fig. 12. For all landing sub-regions, both TRMM and GSMaP consistently show the patterns of M.A.E. at different rain rates for both sides of the T.C. track (Fig. 11). Overall, higher M.A.E. values are found at higher rain

rates, indicating challenges for both satellite datasets in accurately capturing heavy rainfall within T.C. systems. These findings align with the results reported by Yu et al. (2009). Additionally, across AR1, AR2, and AR5, M.A.E. values tend to be greater on the left side of the T.C. track at all rain rates. Conversely, in AR3 and AR4, the areas with lower M.A.E. values vary depending on the rainfall rates, with the left T.C. side for light rainfall (< 45 mm/day) and the right T.C. side for heavy rainfall (> 45 mm/day).

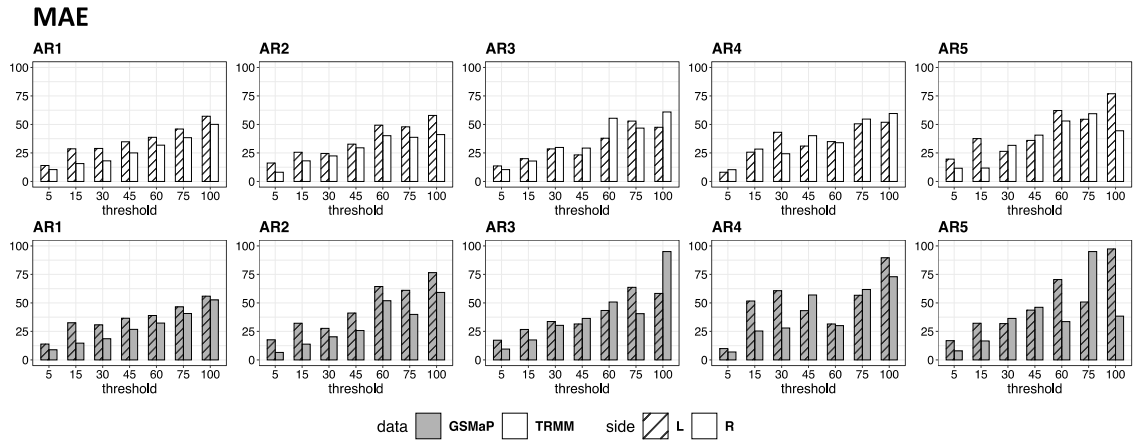

Figure 11. M.A.E. at different rain rates of TRMM (white color) and GSMaP (grey color) for two cases: the left side (diagonal pattern) and the right side (blank pattern) of the T.C. track

Figure 12 (a-d) illustrates the categorical statistical indices of both GSMaP and TRMM for the left and right sides of the T.C. track in different cases of landing sub-regions. Overall, both satellite datasets exhibit a better capability in detecting light rainfall on both sides of T.C.s landing on Vietnam's mainland, except for AR5. Both satellite datasets show similarities for P.O.D. and FAR. The results for P.O.D. are reversed to FAR. In particular, the FAR values decrease as the rain threshold increases (Fig. 12b). The values of P.O.D. are also similar to those in the study of Trinh-Tuan et al. (2019). The P.O.D. values at extreme heavy rainfall thresholds (from about 75 mm/day to 100 mm/day) of GSMaP are higher than those of TRMM in the AR3 and AR4 in our study but exhibited vice versa in the results of Trinh-Tuan et al. (2019). The differences may have come from choosing the research approach and sample data sets. It can be seen that the P.O.D. values are consistently higher on the left side of T.C.s landing in AR1-3 and higher on the right side of T.C.s landing in AR4-5 for almost all rain thresholds.

Additionally, Fig. 12c shows that the satellite data overestimate TC-induced rainfall at almost all rain thresholds, especially for the left side of the T.C. track. However, the magnitudes of F.B.I. are significantly different between cases of landing sub-regions. For the left side of the T.C. track, the F.B.I. values in AR1-3 are smaller than those in AR4-5. On the right side, the F.B.I. values at almost all rain thresholds in cases of T.C. landing in AR1-4 are around 1.0. However, their values are slightly higher in AR5. These findings are consistent with the M.E. results, which indicate a consistently higher positive bias on the left side across all sub-regions, with the most significant biases observed in AR4-5. Besides that, the F.B.I. distribution also relates to the rainfall distribution analysis, demonstrating that heavy rainfall in AR1-3 tends to concentrate on the left side.

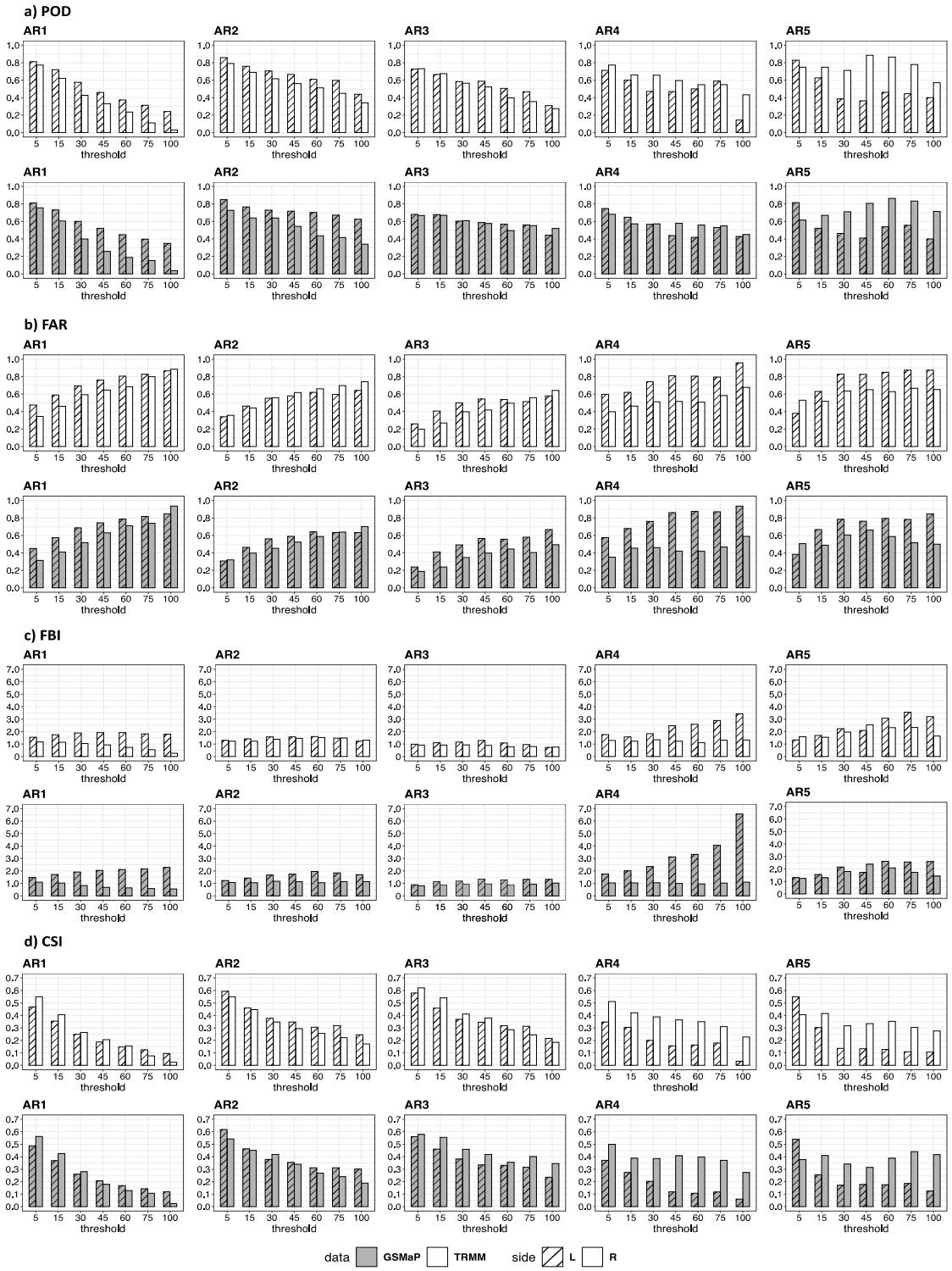

Figure 12. Same as Fig. 11 but for categorical statistical indices: a) P.O.D., b) FAR, c) F.B.I., and d) C.S.I.

In contrast, in AR4-5, it tends to concentrate on the right side (Tran-Minh et. al, 2023). Regarding C.S.I., TRMM, and GSMaP exhibit a decreasing pattern with increasing rainfall thresholds as P.O.D. on both sides of T.C.s landing in AR1-3. This is also pointed out in the study of Bagtasa (2022). However, for T.C.s landing in AR4-5, the C.S.I. values of both datasets on the left side tend to decrease with higher rain intensities, while they remain relatively stable on the right side.

4. Conclusions

This paper has focused on assessing the performance of the TRMM and GSMaP rainfall estimates for T.C.s landing on Vietnam's mainland during the 2000-2019 period. In particular, two groups for detailed evaluations were conducted depending on T.C. intensities and landing sub-regions as follows: (1) Group 1 is based on T.C. intensities, including Tropical Storm (T.S.) for cases with maximum wind speeds ranging from 63-88 km/h, Severe Tropical Storm (S.T.S.) for cases with maximum wind speeds ranging from 89-117 km/h, and Typhoon (T.Y.) for cases with maximum wind speeds of >=118 km/h; (2) Group 2 is based on T.C. landing sub-regions, consisting of five sub-regions labeled as AR1-5.

(1) The results show that TRMM and GSMaP rain products successfully capture the radial distribution of observed T.C. rainfall. The rainfall gradually decreases as the distance from the T.C. center increases, with the highest TC-induced rainfall band typically found within a radius of 100 km from the T.C. center. However, both satellite rainfall products tend to underestimate rainfall when the distance from the T.C. center is relatively close (within 100 km) and overestimate it for greater distances when compared to observations. It leads to positive M.E. dominating Vietnam's mainland stations, irrespective of T.C. intensities and landing sub-regions. Additionally, there is a high homogeneity of the M.A.E. spatial distributions between GSMaP and TRMM, with values generally decreasing as the distance from the coast increases. Notably, irrespective of T.C. intensities and landing sub-regions, the coastal regions of Central Vietnam (AR3-4) consistently exhibit high M.A.E. values, exceeding 50 mm/day, indicating challenges in accurately estimating TC-induced rainfall in these areas for both TRMM and GSMaP datasets.

(2) Significantly, for all T.C. intensities, M.A.E. exhibits a similar pattern between TRMM and GSMaP, with higher values on the left side of the T.C. track when compared to those on the right side. In the cases of different T.C. landing sub-regions, the side of the T.C. track with higher M.A.E. is diverse. In particular, M.A.E. tends to be greater on the left side than on the right side of the T.C. track for almost all T.C. landing sub-regions, except for AR3 and AR4. However, in all cases involving T.C. intensities and T.C. landing sub-regions, higher M.A.E. consistently is found in regions near the T.C. center within 200 km, especially at distances below 100 km for both TRMM and GSMaP. The magnitude of M.A.E. closely aligns with the observed TC-induced rainfall. It indicates that the accuracy of the satellite estimates is influenced by the intensity of TC-induced rainfall, with higher M.A.E. occurring in areas experiencing more significant rainfall amounts.

(3) It is reflected by the P.O.D. values of both TRMM and GSMaP, which generally tend to decrease as rain thresholds increase on both sides of the T.C. track in different cases of landing sub-regions. This means both satellite datasets exhibit a better capability in detecting light TC-induced rainfall. The P.O.D. values are consistently higher on the left side of T.C.s landing in AR1-3 and higher

on the right side of T.C.s landing in AR4-5 for almost all rain thresholds. Besides that, the satellite rain estimates tend to overestimate TC-induced rainfall at almost all rain thresholds, especially on the left side of the T.C. track. However, the magnitudes of F.B.I. are significantly different between cases of landing sub-regions. On the left side of the T.C. track, the F.B.I. values in AR1-3 are smaller than those in AR4-5. While on the right side of the T.C. track, the F.B.I. values of almost all rain thresholds in cases of T.C. landing in AR1-4 are around 1.0. However, their values are slightly higher in AR5, which is consistent with the results of M.E. Regarding the C.S.I. values of both satellite datasets, they show a pattern of decreasing values as the rain thresholds increase for cases of T.C.s landing in AR1-3. However, for T.C. cases landing in AR4-5, the values of C.S.I. on the left side of the T.C. track tend to decrease with increasing rain intensities, while these values remain relatively stable on the right side of the T.C. track.

These results suggest that the performance of satellites in evaluating TC-induced rainfall over Vietnam's mainland depends on TC-induced rainfall intensity. Light rainfall is estimated more accurately than heavy rainfall. As a result, the higher M.A.E. values occur in the coastal areas, where most TC-induced rainfall concentrates, particularly within a 200 km radius from the T.C. center. This presented evaluation remarks on the characteristics of TRMM and GSMaP in estimating TC-induced rainfall, which is helpful for their further uses in building TC-rainfall forecast statistical models for the Vietnam region. However, this study only focused on T.C.s with at least tropical storm (T.S.) intensity, while tropical depressions have also been observed to cause significant rainfall in Vietnam (Nguyen et al., 2016; Olaguera et al., 2023; Yokoi and Matsumoto, 2008). Therefore, it is necessary to evaluate the performance of satellites in capturing typhoon-induced rainfall in the context of tropical depressions in future studies.

Acknowledgments

This study was conducted under the full support of the Vietnam National Project 562 (Grand Number ĐTĐL.CN-59/21), funded by the Vietnam Ministry of Science and Technology.

References

Aonashi K., Awaka J., Hirose M., Kozu T., Kubota T., Aonashi K., Awaka J., Hirose M., Kozu T., Kubota T., Liu G., Shige S., Kida S., Seto S., Takahashi N., Takayabu Y.N., 2009. GSMaP passive microwave precipitation retrieval algorithm: Algorithm description and validation. Journal of the Meteorological Society of Japan, 87A, 119–136. https://doi.org/10.2151/jmsj.87A.119.

Ashouri H., Hsu K., Sorooshian S., Braithwaite D.K., Knapp K.R., Cecil L.D., Nelson B.R., Prat O.P., 2015. PERSIANN-CDR: Daily Precipitation Climate Data Record from Multisatellite Observations for Hydrological and Climate Studies. Bulletin of the American Meteorological Society, 96, 69–83. https://doi.org/10.1175/BAMS-D-13-00068.1.

Bagtasa G., 2022. Assessment of tropical cyclone rainfall from GSMaP and G.P.M. products and their application to analog forecasting in the Philippines. Atmosphere, 13, 1398. https://doi.org/10.3390/atmos13091398.

Bahrami, M., Talebbeydokhti, N., Rakhshandehroo, G., Nikoo, M. R., & Adamowski, J. F., 2023. A fusion-based data assimilation framework for runoff prediction considering multiple sources of precipitation. Hydrological Sciences Journal, 68(4), 614-629. https://doi.org/10.1080/02626667.2023.2180375.

Chen S., Hong Y., Cao Q., Kerstetter P.-E., Gourley J.J., Qi. Y., Zhang J., Howard K., Hu J., Wang J., 2013a. Performance evaluation of radar and satellite rainfalls Chefor Typhoon Morakot over Taiwan: Are remote-sensing products ready for gauge denial

scenario of extreme events? Journal of Hydrology, 506, 4–13. https://doi.org/10.1016/j.jhydrol.2012.12.026.

Chen Y., Ebert E.E., Walsh K.J.E., Davidson N.E., 2013b. Evaluation of TMPA 3B42 daily precipitation estimates of tropical cyclone rainfall over Australia. Journal of Geophysical Research: Atmospheres, 118, 11966–11978. https://doi.org/10.1002/2013JD020319.

Chen S.S., Knaff J.A., Marks Jr.F.D., 2006. Effects of vertical wind shear and storm motion on tropical cyclone rainfall asymmetries deduced from TRMM. Monthly Weather Review, 134, 3190–3208. https://doi.org/10.1175/MWR3245.1.

Chokngamwong R., Chiu L.S., 2008. Thailand Daily Rainfall and Comparison with TRMM Products. Journal of Hydrometeorology, 9, 256–266. https://doi.org/10.1175/2007JHM876.1

Deo A., Walsh K.J.E., 2016. Evaluation of TRMM Multi-satellite Precipitation Analysis during the passage of Tropical Cyclones over Fiji. Journal of Southern Hemisphere Earth Systems Science, 66, 442–456. Doi: 10.22499/3.6604.005.

Deo A., Walsh K.J.E., Peltier A., 2016. Evaluation of TMPA 3B42 Precipitation Estimates during the Passage of Tropical Cyclones over New Caledonia. Theoretical and Applied Climatology, 129(3-4), 711–727. https://doi.org/10.1007/s00704-016-1803-0.

Deo A., Walsh K.J.E., Peltier A., 2017. Evaluation of TMPA 3B42 precipitation estimates during the passage of tropical cyclones over New Caledonia. Theoretical and Applied Climatology, 129, 711–727. https://doi.org/10.1007/s00704-016-1803-0.

Derin Y., Yilmaz K.K., 2014. Evaluation of multiple satellite-based precipitation products over complex topography. Journal of Hydrometeorology, 15(4), 1498–1516. https://doi.org/10.1175/JHM-D-13-0191.1.

Ebert E.E., Janowiak J.E., Kidd C., 2007. Comparison of near-real-time precipitation estimates from satellite observations and numerical models. Bulletin of the American Meteorological Soc., Iety, 88, 47–64. Doi: 10.1175/BAMS-88-1-47.

Habib E., Henschke A., Adler R.F., 2009. Evaluation of TMPA satellite-based research and real-time rainfall estimates during six tropical-related heavy rainfall events over Louisiana, U.S.A. Atmospheric Research, 94, 373–388. https://doi.org/10.1016/j.atmosres/2009.06.015.

Hou A.Y., Zhang S.Q., Silva A.M.da, Olson W.S., Kummerow C.D., Simpson J., 2001. Improving Global Analysis and Short-Range Forecast Using Rainfall and Moisture Observations Derived from TRMM and SSM/I Passive Microwave Sensors. Bulletin of the American Meteorological Society, 82, 659–680. https://doi.org/10.1175/1520-0477(2001)082<0659:IGAASF>2.3.CO;2.

Huang H., Chen F., 2019. Precipitation microphysics of tropical cyclones over the western North Pacific based on GPM DPR observations: A preliminary analysis. Journal of Geophysical Research: Atmospheres, 124, 3124–3142. https://doi.org/10.1029/2018JD029454.

Huffman G.J., Bolvin D.T., Nelkin E.J., 2015. Integrated Multi-Satellite Retrievals for G.P.M. (IMERG) technical documentation. NASA/GSFC Code, 612, 47. http://pmm.nasa.gov/sites/default/files/document_files/IMERG_doc.pdf.

Huffman G.J., Bolvin D.T., Nelkin E.J., Wolff D.B., Adler R.F., Gu G., Hong Y., Bowman K.P., Stocker E.F., 2007. The TRMM Multisatellite Precipitation Analysis (TMPA): Quasi-Global, Multiyear, Combined-Sensor Precipitation Estimates at Fine Scales. Journal of Hydrometeorology, 8, 38–55. https://doi.org/10.1175/JHM560.1.

Joyce R.J., Janowiak J.E., Arkin P.A., Xie P., 2004. CMORPH: A method that produces global precipitation estimates from passive microwave and infrared data at high spatial and temporal resolution. Journal of Hydrometeorology, 5, 487–503. https://doi.org/10.1175/1525-7541(2004)005<0487:CAMTPG>2.0.CO;2.

Kidd C., Levizzani V., 2011. Status of satellite precipitation retrievals. Hydrology and Earth System Sciences, 15, 1109–1116. https://doi.org/10.5194/hess-15-1109-2011.

Kubota T., Shige S., Hashizume H., Aonashi K., Takahashi N., Seto S., Hirose M., Takayabu Y.N., Ushio T., Nakagawa K., Iwanami K., Kachi M.,Okamoto K., 2007. Global precipitation map

using satellite-borne microwave radiometers by the GSMaP Project: Production and validation. IEEE Transactions on Geoscience and Remote Sensing, 45, 2259–2275. Doi: 10.1109/TGRS.2007.895337.

Liu Q., Chiu. L.S., Hao X., Yang C., 2021. Spatiotemporal Trends and Variations of the Rainfall Amount, Intensity, and Frequency in TRMM Multi-satellite Precipitation Analysis (TMPA) Data. Remote Sensing, 13(22), 4629. https://doi.org/10.3390/rs13224629.

Lonfat M., Marks Jr.F.D., Chen S.S., 2004. Precipitation distribution in tropical cyclones using the Tropical Rainfall Measuring Mission (TRMM) microwave imager: A global perspective. Monthly Weather Review, 132, 1645–1660. https://doi.org/10.1175/1520-0493(2004)132<1645:PDITCU>2.0.CO;2.

Nesbitt S.W., Zipser E.J., 2003. The diurnal cycle of rainfall and convective intensity according to three years of TRMM measurements. Journal of Climate, 16, 1456–1475. https://doi.org/10.1175/1520-0442(2003)016<1456:TDCORA>2.0.CO;2.

Nguyen D.Q., Renwick J., McGregor J., 2016. On the presence of tropical vortices over the Southeast Asian sea-maritime Continent region. Journal of Climate, 29, 4793–4800.

Nguyen-Thi H.A., Matsumoto J., Ngo-Duc T., Endo N., 2012. Long-term trends in tropical cyclone rainfall over Vietnam. Journal of Agroforestry and Environment, 6, 89−92.

Okamoto K.I., Ushio T., Iguchi T., Takahashi N., Iwanami K., 2005. The global satellite mapping of precipitation (GSMaP) project. Proc. eedings of the 25th International Symposium on Geoscience and Remote Sensing. Seoul. South Korea. IEEE, 3414–3416.

Olaguera L.M.P., Matsumoto J., Manalo J.A., 2023. The contribution of non-tropical cyclone vortices to the rainfall of the Philippines. International Journal of Climatology, 43(4), 1871–1885.

Pham N.T.T., Vu H.H., 2020. Characteristics of tropical cyclone precipitation system along central coastal region of Vietnam by TRMM and GSMaP data. In: Trung Viet N., Xiping D., Thanh Tung T. (eds) APAC 2019. Springer, Singapore. International conference on Asian and Pacific Coasts, Springer, 87–91. https://doi.org/10.1007/978-981-15-0291-0_13.

Pham-Thanh H., Ngo-Duc T., Matsumoto J., Phan-Van T., Vo-Van H., 2020. Rainfall trends in Vietnam and their associations with tropical cyclones during 1979−2019. The Scientific Online Letters on the Atmosphere, A, 16, 169−174. https://doi.org/10.2151/sola.2020-029.

Pham-Thanh H., van der Linden R., Ngo-Duc T., Nguyen-Dang Q., Fink A.H., Phan-Van T., 2019. Predictability of the rainy season onset date in Central Highlands of Vietnam. International Journal of Climatology, 40, 3072–3086. https://doi.org/10.1002/joc.6383.

Rao G.V., Macarthur P.D., 1994. The SSM/I estimated rainfall amounts of tropical cyclones and their potential in predicting the cyclone intensity changes. Monthly Weather Review, 122, 1568−1574.

Rodgers E.B., Adler R.F., Pierce H.F., 2000. Contribution of tropical cyclones to the North Pacific climatological rainfall as observed from satellites. Journal of Applied Meteorology and Climatology, 39, 1658−1678.

Roy P., Rao T.N., 2022. Precipitation Characteristics of Cyclonic Disturbances over the South Asia Region as Revealed by TRMM and G.P.M. Journal of Climate, 35, 4943–4957. https://doi.org/10.1175/JCLI-D-21-0774.1.

Sorooshian S., Hsu K-L., Gao X., Gupta H.V., Imam B., Braithwaite D., 2000. Evaluation of PERSIANN system satellite-based estimates of tropical rainfall. Bulletin of the American Meteorological Society, 81, 2035–2046. https://doi.org/10.1175/1520-0477(2000)081<2035:EOPSSE>2.3.CO;2.

Sun Q., Miao C.Q., Duan Q.H., Ashouri H.S., Sorooshian S., Hsu K.L., 2018. A review of global precipitation data sets: Data sources, estimation, and intercomparisons. Reviews of Geophysics, 56, 79–107. https://doi.org/10.1002/2017RG000574.

Sutton J.R.P., Jakobsen A., Lanyon K., Lakshmi V., 2022. Comparing Precipitation during Typhoons in the Western North Pacific Using Satellite and In Situ

Observations. Remote Sensing, 14, 877. https://doi.org/10.3390/rs14040877.

Tran-Minh H., Vu-Thanh H., Pham-Thi-Thanh N., Pham-Thanh H., 2023. Characteristics of rainfall distribution induced by tropical cyclones making landfall over Vietnam using GSMaP satellite rainfall data. Vietnam Journal of Hydrometeorology, 748, 64–76. Doi: 10.36335/VNJHM.2023(748).64-76 (in Vietnamese).

Tran-Quang D., Pham-Thanh H., Vu T., Kieu C., Phan-Van T., 2020. Climatic Shift of the Tropical Cyclone Activity Affecting Vietnam's Coastal Region. Journal of Applied Meteorology and Climatology, 59, 1755–1768. https://doi.org/10.1175/JAMC-D-20-0021.1.

Trinh-Tuan L., Matsumoto J., Ngo-Duc T., Nodzu M.I., Inoue T., 2019. Evaluation of satellite precipitation products over Central Vietnam. Progress in Earth and Planetary Science, 6, 54. https://doi.org/10.1186/s40645-019-0297-7.

Ushio T., Sasashige K., Kubota T., Shige S., Okamoto K., Aonashi K., Inoue T., Takahashi N., Iguchi T., Kachi M., Oki R., Morimoto T., Kawasaki Z., 2009. A Kalman filter approach to the Global Satellite Mapping of Precipitation (GSMaP) from combined passive microwave and infrared radiometric data. Journal of the Meteorological Society Japan, 87A, 137–151. https://doi.org/10.2151/jmsj.87A.137.

Wilks D.S., 2006. Statistical Methods in the Atmospheric Sciences, 2nd ed., International Geophysics Series, Academic Press. San Diego. California. U.S.A., 91, 627p.

Yang S., Surratt M., Whitcomb T.R., Camacho C., 2024. Evaluation of IMERG and GSMaP for tropical cyclone applications. Geophysical Research Letters, 51, e2023GL106414. https://doi.org/10.1029/2023GL106414.

Yokoi S., Matsumoto J., 2008. Collaborative effects of cold surge and tropical depression-type disturbance on heavy rainfall in central Vietnam. Monthly Weather Review, 136, 3275–3287.

Yu Z., Wang Y., Xu H., Davidson N., Chen Y., Chen Y., Yu H., 2017. On the relationship between intensity and rainfall distribution in tropical cyclones making rainfall over China. Journal of Applied Meteorology and Climatology, 56, 2883–2901. https://doi.org/10.1175/JAMC-D-16-0334.1.

Yu Z., Yu H., Chen P., Qian C., Yue C., 2009. Verification of Tropical Cyclone-Related Satellite Precipitation Estimates in Mainland China. Journal of Applied Meteorology and Climatology, 48, 2227–2241. https://doi.org/10.1175/2009JAMC2143.1.

Yue H., Gebremichael M., Nourani V., 2022. Evaluation of Global Forecast System (G.F.S.) Medium-Range Precipitation Forecasts in the Nile River Basin. Journal of Hydrometeorology, 23, 101–116. https://doi.org/10.1175/JHM-D-21-0110.1.

Zhao D.J., Gao W.H., Xu. H.X., Yu Y.B., Chen L.S., 2022. A modeling study of cloud physical properties of extreme and non-extreme precipitation in landfalling typhoons over China. Atmospheric Research, 277. https://doi.org/10.1016/j.atmosres.2022.106311.

Appendix A. Statistical index formulas

The contingency table (Table A1) is used to compute four commonly categorical statistics, including Probability of Detection (P.O.D.), False Alarm Ratio (FAR), Frequency Bias Index (F.B.I.), and Critical Success Index (C.S.I.).

Table A1. Contingency Table

	Observed rainfall ≥ threshold	Observed rainfall < threshold
Satellite-based rainfall ≥ threshold	Hits	False alarms
Satellite-based rainfall < threshold	Misses	Correct negatives

The Probability Of Detection (P.O.D.) is sensitive to hits and suitable for rare events. The optimal value of P.O.D. is 1.

$$\mathrm{POD} = \frac{\mathrm{hits}}{\mathrm{hits} + \mathrm{misses}} \quad \text{(A1)}$$

The False Alarm Ratio (FAR) is sensitive to false alarms. The optimal value of FAR is 0.

$$\mathrm{FAR} = \frac{\text{false alarms}}{\text{hits} + \text{false alarms}} \quad \text{(A2)}$$

The Frequency Bias Index (F.B.I.) shows the ratio of the frequency of estimated satellite rain events to the frequency of observed rain events. The estimates show a tendency to overestimate (F.B.I.>1) or underestimate (F.B.I.<1) the observations. The ideal value of F.B.I. is equal to 1.

$$\mathrm{FBI} = \frac{\text{hits} + \text{false alarms}}{\text{hits} + \text{misses}} \quad \text{(A3)}$$

The Critical Success Index (C.S.I.) is considered as the measurement of the agreement between estimates and observations. The ideal value of C.S.I. is equal to 1.

$$\mathrm{CSI} = \frac{\text{hits}}{\text{hits+false alarms+misses}} \quad \text{(A4)}$$

The Mean Error (M.E.) measures the average error between satellite rainfall estimations and observations. It indicates a tendency to overestimate (ME > 0) or underestimate (ME < 0) the observations. The ideal value of M.E. is equal to 0. The range of M.E. is (-∞,+∞).

$$\mathrm{ME} = \frac{1}{n}\sum_{i=1}^{n}(S_i - O_i) \quad \text{(A5)}$$

The Mean Absolute Error (M.A.E.) shows the average error magnitude between estimations and observations. The ideal value of M.A.E. is equal to 0. The range of M.A.E. is (0,+∞).

$$\mathrm{MAE} = \frac{1}{n}\sum_{i=1}^{n}|S_i - O_i| \quad \text{(A6)}$$

where S_i are value of satellite rainfall estimations, O_i are value of rainfall observations, and n is sample number.